Nuclear Inst. and Methods in Physics Research B 438 (2019) 70–76

Contents lists available at ScienceDirect

Nuclear Inst. and Methods in Physics Research B

journal homepage: www.elsevier.com/locate/nimb

Actinides AMS on the VEGA accelerator

M.A.C. Hotchkis[a,*], D.P. Child[a], M.B. Froehlich[b], A. Wallner[b], K. Wilcken[a], M. Williams[c]

[a] Australian Nuclear Science and Technology Organisation, Sydney, Australia
[b] Australian National University, Canberra, Australia
[c] University of Wollongong, Wollongong, Australia

ARTICLE INFO

Keywords:
Accelerator mass spectrometry
Actinides
Plutonium
Uranium

ABSTRACT

The VEGA 1MV accelerator at ANSTO is designed to be a highly versatile AMS instrument. In this paper we focus on describing those aspects of the system that are designed to optimise its performance for actinides isotopic analysis, in particular the implementation of fast isotope cycling and multiple isotope detection methods to enable isotope detection across a wide range of rates and currents. Charge state yields are reported in the energy range from 0.3 to 1.0 MeV with helium gas stripping, showing that the highest yield for the 3+ charge state occurs around 1 MeV and exceeds 40%. Accuracy and precision for uranium isotope ratios are shown to approach 1% over a wide range of concentrations and isotope ratios. The ionisation efficiency for plutonium is shown to exceed 3%, leading to overall detection efficiency over 1%. In the absence of background, this leads to sub-attogram detection limits for several Pu isotopes including ^{244}Pu.

1. Introduction

Analysis of actinides by Accelerator Mass Spectrometry (AMS) is now finding a wide range of applications. At ANSTO, our work in this area encompasses applications with a variety of analytical requirements in terms of sensitivity, measurement precision, the range of isotopes of interest, and a very wide range of isotope concentrations.

For our work in nuclear safeguards and nuclear forensics [1–3] the requirements [4] include (i) sub-femtogram sensitivity for plutonium isotopes and for 'minor' uranium isotopes (^{233}U, ^{236}U), (ii) < 1% precision in isotope ratios for 'major' uranium isotopes (^{234}U, ^{235}U, ^{238}U), and (iii) uranium blank level < 0.1 ng for cotton wipes (swipe samples). These requirements pose several challenges which are also compounded by, in many instances, a lack of fore-knowledge of the amount of U and Pu that may be present in the samples, thereby adding risks of cross-contamination both in sample preparation and in analysis.

Monitoring and studying radiologically contaminated sites poses similar challenges with highly variable actinide concentrations [5–8]. Good precision in Pu isotope ratios provides the means to trace and differentiate sources, and delineate the global and regional characteristics of fallout [6]. Very high sensitivity (< 0.1 fg Pu) enables radioecological studies [5,9] in areas with environmentally-relevant levels of contamination, even for the case of plutonium which is expected to have very low but non-zero uptake into flora and fauna [10].

We are using fallout actinides in geochronology and environmental science, in particular fallout Pu in combination with ^{210}Pb and/or ^{14}C for sedimentation and depositional histories [11–14]. Analytical requirements are less stringent than in the aforementioned cases. However, high sensitivity enables detection of additional fallout species which may provide additional information, as in the case of ^{236}U fallout [14].

As part of a project aimed at the observation of radionuclides of interstellar origin in deep sea ferro-manganese crusts and sediments [15,16], we have tested the sensitivity of our AMS system for ^{244}Pu detection. Ultimately, in the absence of background sources, AMS sensitivity is limited by ion source efficiency and beam transmission. In the case of ^{244}Pu, interference from nearby masses is not expected to be significant, as nearby mass species have generally very low abundance. In addition to ^{244}Pu, there is interest in other rare species with half-lives greater than 1 Ma, such as ^{247}Cm. In both cases, the project also requires the capability to measure a range of other Pu, Am and Cm isotopes for normalisation and for assessment of global fallout contributions.

The recently-installed VEGA 1MV accelerator system at ANSTO has been designed to provide optimum performance for actinides and to meet the above range of requirements. In a previous paper [17], the overall system was described, including preliminary performance results ^{10}Be, ^{14}C, ^{26}Al and actinides. Fig. 1 shows the VEGA 1MV AMS with specifications of the major elements. In this paper we describe details of the system as applied to actinides analysis, addressing the

* Corresponding author.
E-mail address: mah@ansto.gov.au (M.A.C. Hotchkis).

https://doi.org/10.1016/j.nimb.2018.07.029
Received 31 January 2018; Received in revised form 26 July 2018; Accepted 29 July 2018
Available online 01 September 2018

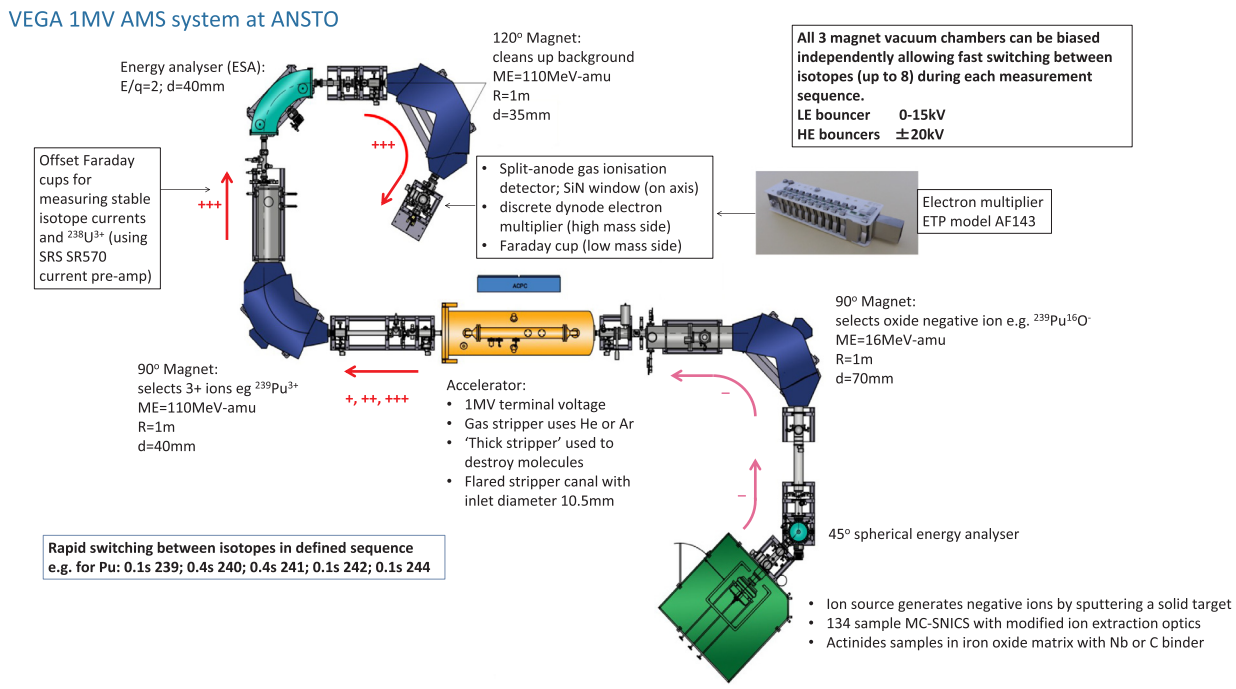

Fig. 1. Schematic of the VEGA AMS system including details relevant to actinides analysis. The system was manufactured by National Electrostatics Corporation (NEC) [18].

performance requirements of the above-mentioned projects. We report results demonstrating those performance characteristics.

2. Beam transmission and charge state distributions

Actinides are injected into the accelerator as monoxide negative ions. Previous work [19,17] has shown that helium gas stripping, to the 3+ charge state, provides the optimum charge state yield in the energy range of the VEGA accelerator. Since our previous publication [17], the gas stripper canal was modified to improve the tuning conditions used for radiocarbon analyses. The stripper canal internal diameter, and that of the preceding two entrance apertures, has been enlarged from 8 mm to 10.5 mm. The canal is flared towards the exit end, with exit diameter increased from 9.5 mm to 12 mm, and the flaring extends to the final exit aperture which now has a diameter of 17 mm. The effect of this change has primarily been to improve flat-topping and ease of tuning, rather than having a significant effect on overall transmission. No detrimental impact has been observed. Results reported here were obtained using the new gas stripper arrangement.

We have measured charge state yields from 0.3 to 1.0MV terminal voltage with uranium oxide negative ions, injected at 60 keV. The charge state yield is calculated as the beam intensity for a particular charge state, in particle amps, measured after the first high energy (HE) analysing magnet, divided by the injected beam intensity in amps. The system, including the gas stripper pressure, was tuned initially for maximum 3+ beam transmission. For measurement of other charge states, only the quadrupole at the exit of the HE tube and the HE analysing magnet were adjusted.

In Fig. 2 the charge state yields are shown as a function of energy, bridging a gap in published data between 0.5 and 1.0 MeV. Clear discontinuities are evident between the datasets which need explanation. The discontinuities between the data from the three different accelerators can in part be attributed to non-optimal beam transmission at terminal voltage settings below the designed optimum. For VEGA measurements below 0.6 MeV, shorting rods were used to improve beam optics (1/3 of low energy (LE) tube shorted); also VERA (Vienna) [20] used shorting for some of the data range shown. While use of shorting rods can improve transmission in the LE tube, the geometries

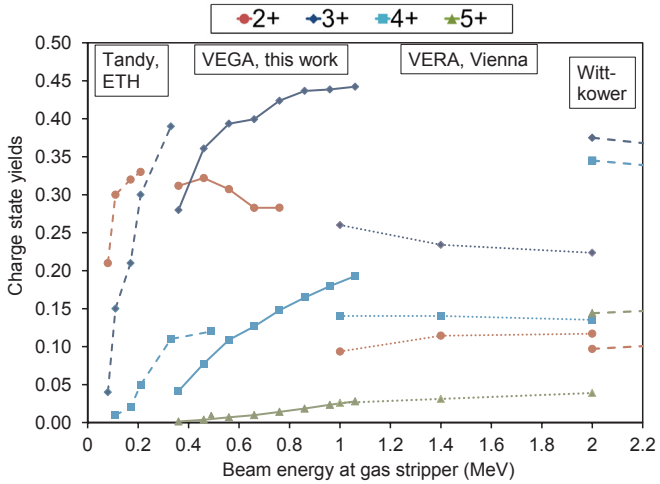

Fig. 2. Charge state yields vs. energy, as measured on the Tandy [19], VEGA (this work) and VERA [20] accelerators, and data at higher energy (Wittkower) [21]. The VERA data were measured as charge state fractions and have been normalised here to match their estimate of the charge state yield for the 3+ at 1MV.

of the stripper canals and HE tubes are critical in achieving maximum transmission through the HE side and may not be optimised in each accelerator for the energy range and particle type here. The data from Wittkower and Betz [21] were acquired with an apparatus using an external beam and so are not subject to the same effects.

Our data show that the 3+ yield continues to climb with increased energy, as expected from the lower energy data [19]. At 0.7MV, where we are able to measure all major charge states except the 1+, the sum of the measured charge states accounts for nearly 90% of the injected beam, demonstrating that there is limited scope for further gains from improved geometry at this or higher voltages. The trends of the data in Fig. 2 are consistent with the peak yield for the 3+ charge state occurring at around 1 MeV.

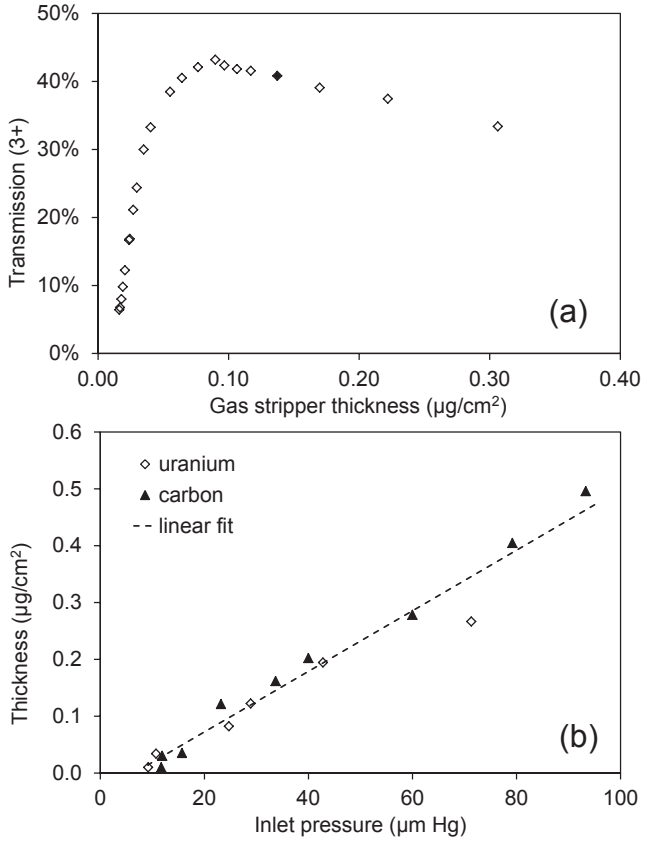

Fig.3. (a) Transmission as a function of stripper pressure at 0.68MV for thorium oxide injection. The data point with the filled symbol indicates the gas thickness generally used for actinides analysis to ensure destruction of molecular interferences (see discussion below). (b) Determination of the gas thickness versus the stripper gas pressure reading. The pressure gauge has an offset of around 8 μm Hg.

The beam transmissions measured above were recorded with gas pressure set to maximise the 3+ transmission. Transmission is plotted versus gas stripper thickness for ThO^- ion injection in Fig. 3(a). Also shown in Fig. 3(a) is the stripper thickness required to ensure molecular background suppression; this is discussed further below. The relationship between the gas stripper thickness and the pressure, as read on a gauge on the inlet pipe to the canal, is shown in Fig. 3(b). This relationship was determined by measuring how far the beam was shifted after analysis as the gas pressure was increased. Following each increment of the gas pressure, the first analysing magnet was adjusted to re-centre the beam at the image position. In addition, the ESA was adjusted to re-centre the beam at its image position. The required increments of the magnetic and electrostatic fields were found to be consistent with each other and were used to determine the energy shift of the beam. The SRIM code [22] was used to derive the change in gas thickness. This was done with both carbon and actinide beams and consistent results were obtained.

3. Multi-isotope capability and isotope measurement techniques

To ensure good precision and efficiency, fast isotope cycling is implemented on VEGA for all combinations of isotopes that may be required. For actinides, multiple isotopes need to be counted in the same detector and this is achieved in our system with electrostatic bouncing applied not only to the injection magnet but also to both high energy analysing magnets. A typical isotope cycle is around one second (see Fig. 1); times are adjusted according to expected isotope abundance or particular analysis needs. The HE bouncer system has a response time of around 1.0 ms, depending on voltage change. In the isotope measurement sequence, a switching and settling time of 5 ms per isotope is allowed for, hence a total switching time of 25 ms or about 2.5% per cycle.

In our tuning procedure, a pilot beam of thorium is used, injected as ThO^-. The injection magnet is tuned with an appropriate voltage applied to the low energy bouncer (which has a unipolar power supply), so that the magnet does not need further adjustment to inject isotopes required for measurement. HE magnets are also tuned with the pilot beam and are then kept fixed. The terminal voltage and HE electrostatic analyser are scaled to transmit the central mass in the range of isotope masses of interest. This need not be an integer value; for example, for Pu, the masses of interest are usually 239, 240, 241, 242 and 244, so the central mass is 241.5. The HE bouncers are bipolar so this procedure minimises the required voltages. The voltage range is ± 20 kV, enabling analysis of up to 8 masses around mass ~240 at 1MV with 3+ ions. In the plutonium example, all bouncer voltages are tuned for each individual isotope, using a suitable standard, except in the case of ^{241}Pu, where bouncer voltages are interpolated from 240 and 242 settings.

Rare species such as the plutonium isotopes are counted in a parallel-plate ionisation chamber with a 75 μm SiC gas window. An energy spectrum showing separation of $^{240}Pu^{3+}$ ions from other species is shown in Fig. 4. As species arriving at the detector are constrained by beam optics to have matching mass-to-charge ratio, we can infer that the other species observed are likely to be $^{80}Se^{1+}$ and $^{160}Dy^{2+}$, or molecular species of the same mass and charge. Low rates of 1+ and/or 2+ ions are frequently observed in $^{240}Pu^{3+}$ spectra, and also in $^{234}U^{3+}$ and $^{242}Pu^{3+}$ spectra, but not at rates that cause interference. In the case of $^{243}Am^{3+}$, we do find high rates of 2+ ions. Their effect is minimised by implementing pile-up rejection in the electronics. A pulser signal is used for dead-time correction.

In the case of uranium isotopes, the terminal voltage and HE electrostatic analyser are typically set to transmit mass 235.5 on-axis at zero HE bouncer voltages. Note that this choice is arbitrary and does not impact the effectiveness of the system for background suppression (for example, for suppression of ^{235}U when measuring ^{236}U). The set-up required for uranium isotope measurements is considerably more complicated than for Pu and other low-abundance species. In Table 1 a range of sample types are listed with estimates of the consequent isotope beam currents and/or counting rates. Factoring in the need to measure process blanks for swipes at the 0.1 ng level, the uranium contents span seven orders of magnitude, with ^{236}U content potentially spanning an even wider range.

The first issue to note with regard to Table 1 is that the wide range of concentrations poses risks of cross-contamination and thus necessitates having several separate laboratory spaces available for processing such materials. Samples with known risks are screened, usually by

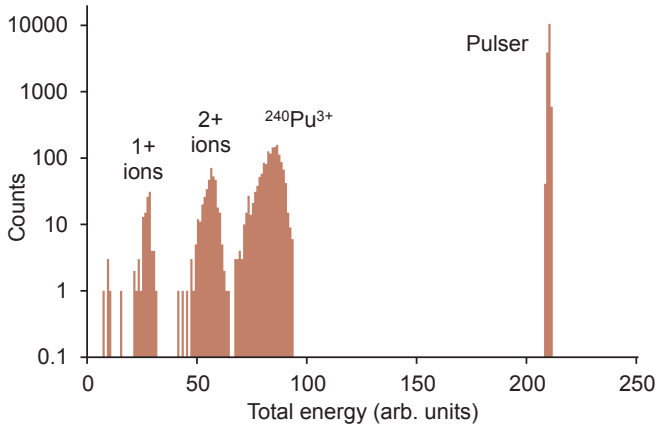

Fig. 4. Detector energy spectrum for $^{240}Pu^{3+}$, for plutonium extracted from a soil sample. The energy resolution (FWHM) is 11%.

Table 1
U range of materials and corresponding isotope rates/currents. ^{233}U is usually added as spike so its count rate is predictable. cps = counts per second.

Sample types and typical contents						
	U ore	U forensic sample	Soil/sediment	Soil/sediment (contaminated)	Swipe (clean)	Swipe (dirty)
Typical U content*	1000 μg	1000 μg	1 μg	1 μg	0.001 μg	up to 0.1 μg
Range of 236/238 ratio	10^{-13}–10^{-10}	10^{-10}–10^{-6}	10^{-10}–10^{-7}	10^{-9}–10^{-5}	10^{-9}	10^{-9}–10^{-4}
Range of ^{236}U content	0.1–100 fg	100–1,000,000 fg	0.1–100 fg	1–10,000 fg	0.001 fg	0.1–10,000 fg
Corresponding isotope currents (as particle current) or counting rates						
^{238}U	100,000 pA	100,000 pA	100 pA	100 pA	0.1 pA	10 pA
^{235}U**	1000 pA	1000 pA	1 pA	1 pA	7000 cps	0.1 pA
^{234}U**	5 pA	5 pA	0.005 pA	0.005 pA	35 cps	3500 cps
^{236}U	0.07–70 cps	70 cps–0.1 pA	0.07–70 cps	0.7–700 cps	0.0007 cps	0.007–700 cps

* Potential content derived from sample material processed for analysis, if not diluted.
** Estimate based on natural isotope ratios; in some cases, real sample ratios may differ from natural values by a factor of ten.

gamma spectrometry to indicate irradiated materials, or by XRF for high U content. On the ANSTO site, a radioanalytical lab is used for gamma analyses on samples from contaminated sites and also a separate active sample-capable laboratory is used to perform a variety of analyses on forensic samples. Sub-sampling and/or dilution may be required before such samples are transferred from these labs to our AMS labs. Within our AMS facility, we have two clean labs: a 'cold' lab which can take samples with U contents up to about 1 μg and ^{236}U up to about 1 pg, while our 'warm' lab takes any samples expected to be higher than this. Neither AMS laboratory is classified as radiological and so are only suitable for samples classed as non-active.

The next issue to consider is the potential for cross-contamination in the ion source. In our experience with actinides, for a given isotope in a single sample set, a concentration range of not more than 4 orders of magnitude is tolerable. Beyond that range, samples must be segregated and the ion source cleaned between such operations. In practice, we believe there is a long-term risk of source contamination, if we were to run U ore-type samples regularly, as this could compromise our U swipe blanks. As a result, we do not currently run pure uranium oxide samples on this system and the tests we have done with ores have mainly been done with diluted samples. Forensic-type samples, which may also have large amounts of uranium available for analysis, are if necessary subsampled for analysis (total U $<$ 10 μg).

Finally there is the issue of how to measure the required isotopes given the range of currents and counting rates.

1. Low abundance isotopes (^{236}U, the ^{233}U spike and in some cases ^{234}U) can be measured in the gas ionisation counter (GIC), which is suited to rates up to about 5000 counts per second. Detector electronic and data acquisition dead time is monitored and corrected for.
2. At the other end of the scale, ^{238}U with currents > 10 pA can be measured in the off-axis Faraday cup on the high-mass side after the first HE analysing magnet. An appropriate extra voltage is applied to the HE bouncer on this magnet to 'push' the mass 238 beam into the cup. Without the extra voltage, the cup would need to be too close to the on-axis beams. Using the SRS model SR570 current pre-amp on this Faraday cup, currents above 10pA can be measured reliably and reasonably efficiently. Using the 20 pA/V range, 150 ms measurement time is required. While such a pre-amp is in principle able to measure much lower currents than 10 pA, the time constant on lower current ranges is such that it ceases to be an efficient method for measuring beams pulsed by the bouncer, as long integration times would be needed.
3. To bridge the gap between 5000 cps and 10 pA current, a discrete-dynode electron multiplier (EM) (ETP model AF143) [23] is used, in current amplifying mode. The voltage on the dynode chain is adjusted to achieve a gain in the range 10^5–10^7, ensuring the resulting currents are well within range of the NEC-supplied Precision Pulse Current Integrators.
4. For uranium isotope analysis, the EM is positioned off-axis on the high-mass side after the final analysing magnet. The final magnet setting is adjusted to put mass 234 on axis, while the first analyser remains on the mass 235.5 setting. For samples containing nanogram quantities of uranium, ^{233}U, ^{234}U and ^{236}U are counted in the ion chamber, and ^{235}U and ^{238}U are deflected into the EM. For samples containing microgram quantities of uranium, ^{234}U and ^{235}U are deflected into the EM, and ^{238}U is deflected into the Faraday cup after the first magnet (as in (2) above). In all cases, the cycle time is typically one second. The EM feeds currents to the Precision Pulse Current Integrator; to compensate for the difference in currents of the two isotopes measured in this device during the cycle, the integration time is usually set to 1 ms for the high-abundance isotope (235 or 238) and 100 ms for the other (234 or 235), hence both can be measured without changing the selected range.

4. Isotope ratio measurement performance

A series of uranium standards (see Table 2) have been made up in a range of concentrations, from 1 to 500 ppm U, to verify the performance of the system over the required wide range of isotope abundancies. Each cathode contains around 5 mg iron oxide; hence the highest amount, per cathode, of uranium is 2.5 μg, of ^{236}U is 3 pg. Generally, the ratio measurements show excellent internal precision (~1%) for ^{234}U/^{238}U, ^{235}U/^{238}U and ^{236}U/^{238}U ratios, unless limited by counting statistics. Fig. 5 shows typical data; here the standard deviation of the normalisation factor is 1.45%, compared to an average uncertainty of 1.39%. However, when operated with high gain (10^7), the EM shows both a current dependence and a gain drift with time, as shown in Fig. 6. Selected standards are used to evaluate these effects and apply appropriate corrections. After applying corrections, the standard deviation of the 235/238 data in Fig. 6 is 0.26%.

To evaluate both precision and accuracy, the results obtained for the set of standards were compared to the certified values. Fig. 7 shows the relative deviations from certified values for this sample set. This includes datasets obtained (i) with ^{234}U and ^{236}U counted in the GIC while both ^{235}U and ^{238}U are in the EM, for low-U samples (at two different EM gain settings), and (ii) with ^{236}U in GIC, ^{234}U and ^{235}U in EM, and ^{238}U in the FC, for medium-level-U samples. Sample results

Table 2
Uranium atom ratios and concentrations for the standards used in this work.

	234/238	235/238	236/238	Concentrations used (ppm by weight)
NIST 4321c	5.17E−05	0.71%	< 1E−08 [1]	1, 10, 50, 500
NBL U0002	1.60E−06	0.02%	< 1E−07	1, 10, 50, 500
NBL U005-A	3.42E−05	0.51%	1.19E−05	1, 10
NBL U010	5.47E−05	1.01%	6.88E−05	1, 10
NBL U030-A	2.87E−04	3.14%	6.18E−06	1, 10

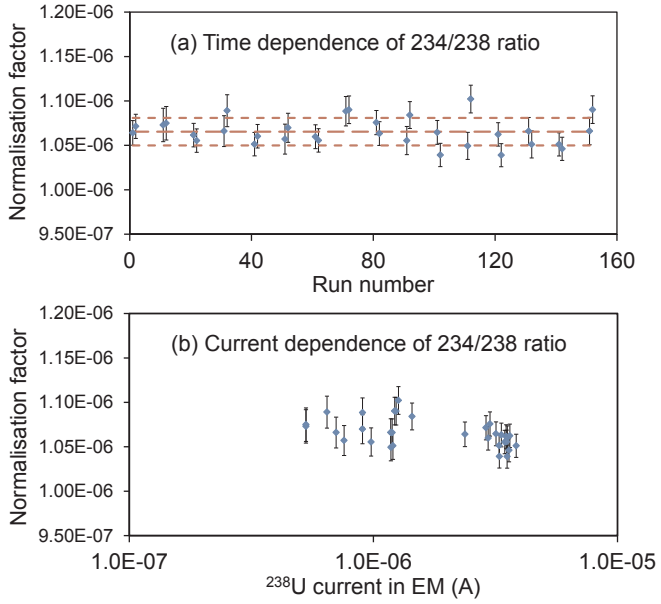

Fig. 5. (a) Time and (b) current dependence of the normalisation factor for 234/238 ratio for the NIST4321C standards at 1 and 10 ppm. ^{234}U is counted in the gas ionisation detector while both ^{235}U and ^{238}U are in the EM. The normalisation factor is defined as the (measured ratio)/(expected ratio) and is approximately equal to 1/(EM gain). Errors are statistical errors in ^{234}U counts. The mean ± σ lines are shown in (a). Measurements span a six hour period.

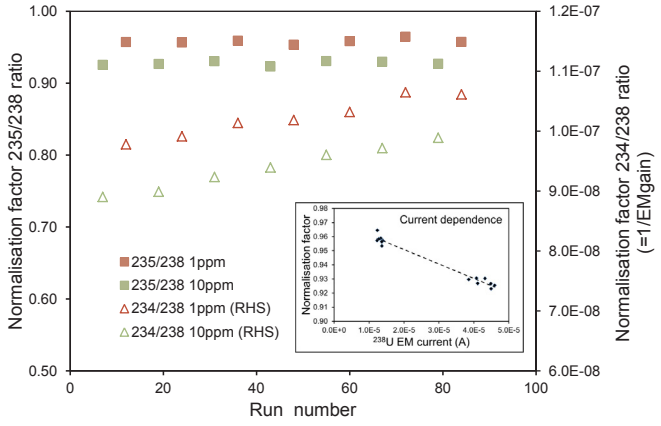

Fig. 6. Normalisation factors for ^{235}U/^{238}U and ^{234}U/^{238}U ratio for the NIST4321C standard at 1 and 10 ppm. Compared to Fig. 5, the EM voltage was increased to improve the sensitivity for ^{235}U in highly depleted samples. Inset: the current dependence of the 235/238 ratio, caused by non-linear response of the EM at high gain.

that were used for normalisation are not included in these results. Where necessary, the normalisation samples were used to determine corrections that were applied for gain drift and non-linearity of the EM. In addition, the contribution from background uranium present in the samples has been subtracted, based on measured U isotopes in iron oxide blanks. High precision (< 1%) is clearly achievable unless limited by counting statistics. However, further work is required to achieve good accuracy across the range of isotopes and concentrations. We are further investigating the variability of uranium background contributions in order to solve this problem, which particularly affects the low concentration samples.

5. Abundance sensitivity and detection limits

In earlier works [19,24], it has been shown that a significant source of interference for actinides when measured in the 3+ charge state can come from surviving UH^{3+} molecular ions, affecting both ^{236}U and ^{239}Pu detection. It is necessary to ensure that an adequate stripper gas pressure is attained to destroy the molecules; we have made similar checks on our system and established the abundance sensitivity limits as listed in Table 3. For the ^{233}U, ^{239}Pu and ^{240}Pu limits, we used samples doped with microgram quantities of thorium and uranium to establish the relevant isotope limits. The 236/235 limit was determined using a sample with known low ^{236}U/^{238}U ratio (containing uranium extracted from the ore ANU-103, with ratio 1.03×10^{-12} [25]). The mass 237 limit (in presence of ^{238}U) is an estimate based on interpolated tuning settings and required narrow slit settings after the HE ESA. In all other cases, slit settings are set to transmit > 95% of ions.

In addition we have investigated Pu absolute isotope detection limits in the absence of added uranium, using a ^{242}Pu spike sample. In Fig. 8, the measured isotope amounts are plotted against gas stripper thickness for $^{239\text{-}241}$Pu. This shows that a higher gas pressure is required to eliminate interferences at mass 240 than at 239 or 241. These data and the abundance sensitivity results are not consistent with uranium as the source of mass 240 background; another species must be responsible, which we have not yet been able to identify. The samples used were of high purity, hence the rate of 1+ and 2+ ions were very low and not a source of interference. We ran a test with carbon samples and found they do not give a high rate at mass 240, so it is unlikely that carbon clusters (e.g. C_{20}^{3+}) are responsible.

The main data set in Fig. 8 was obtained with 10 min runs at each stripper setting. Additionally, a long run (8 h on one sample) was performed with a stripper thickness of 0.18 μg/cm^2 to test the ultimate limit for each isotope. The amounts of isotopes present for masses 239–241 were found to be at 9 ag, 0.4 ag and 0.2 ag respectively. These amounts significantly exceed the amounts calculated from the activity limits specified on the spike material certificate (NIST SRM 4334H). An unspiked pure iron oxide material was also run for a similar time and gave similar counting rates and hence we conclude that the levels measured represent laboratory, material or ion source contamination.

6. Overall efficiency and ^{244}Pu detection limit

A more detailed study has been undertaken of isotope sensitivity for the case of ^{244}Pu, to address the requirements of nuclear astrophysics research [15,16]. In the absence of ion interferences in the detector, the sensitivity is determined by: (i) charge state yield (see above); (ii) beamline transmission, > 95% in our system; and (iii) the ion source efficiency, to which we now turn our attention.

The ion source on the VEGA accelerator is a 134-sample MC-SNICS source supplied by NEC. Its design is modified from earlier versions and incorporates findings from earlier work [26–28] to improve vacuum and to reduce beam emittance. The bias (pre-acceleration) voltage is applied across a single gap without field grading; a large diameter beamline insulator is used, enabling better source pumping (1×10^{-6} Pa base pressure). Typically for running actinides, the cathode voltage is 6 kV and total source output adjusted to around 100μA (primarily $^{16}O^-$ from the iron oxide targets), leading to cathode current 1.0–1.2 mA. For Pu analysis at ANSTO, the iron oxide is mixed with niobium powder, and loaded into aluminium cathodes.

In one test to evaluate overall efficiency, 25.5 fg (6.35×10^7 atoms) ^{242}Pu spike (NIST SRM 4334H) was dispersed in 11 mg of iron oxide, mixed with an equal mass of niobium powder and split into 2 cathodes. The exact mass split between the two cathodes was not recorded. Their performance is shown in Fig. 9. The pair were run to exhaustion, for a combined time of 22 h, yielding a total of 40,328 counts ^{242}Pu and 1 count ^{244}Pu. With the cycle used, the overall efficiency is calculated to be 1.3%. Total beam transmission, measured with a Th tuning beam, was 39.6%; therefore we deduce an ion source efficiency of 3.2% for the formation of PuO^- ions.

The single count of mass 244 detected corresponds to 0.035 ag

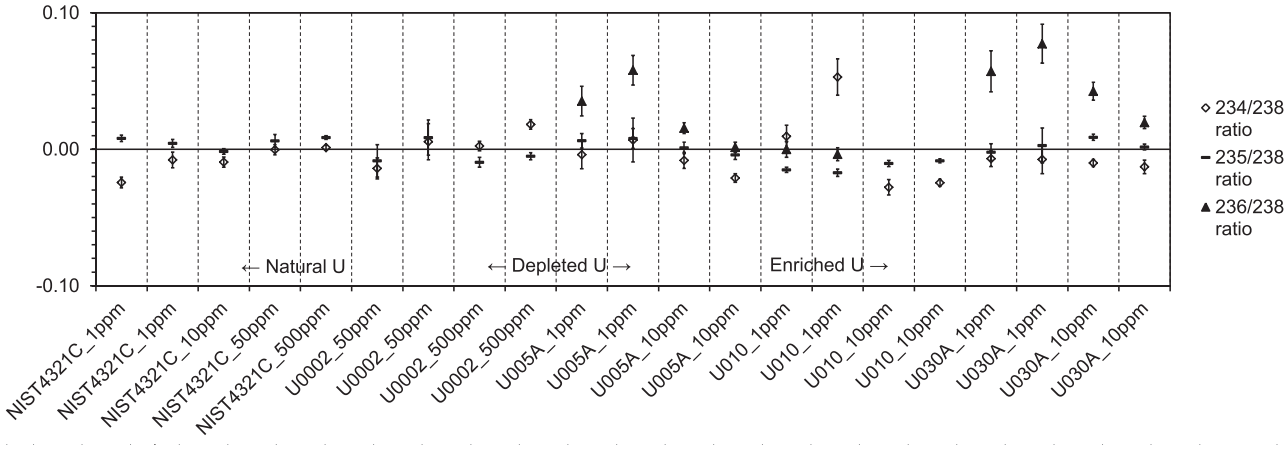

Fig. 7. Relative deviations in U isotope ratios for a set of U standards prepared with concentrations in the range 1–500 ppm.

Table 3
Abundance sensitivities for a range of actinides species, relative to major isotope present.

Isotope or species ratio	Sensitivity limit
$^{233}U/^{232}Th$	2.7×10^{-9}
$^{236}U/^{235}U$	1.8×10^{-9}
$^{237}X/^{238}U$	2×10^{-13}
$^{233}U/^{238}U$	2×10^{-14} *
$^{239}Pu/^{238}U$	1.3×10^{-9}
$^{240}Pu/^{238}U$	$< 5.0 \times 10^{-10}$

* Limited by ion source background due to use of thorium for beam tuning (using samples with 1% Th content).

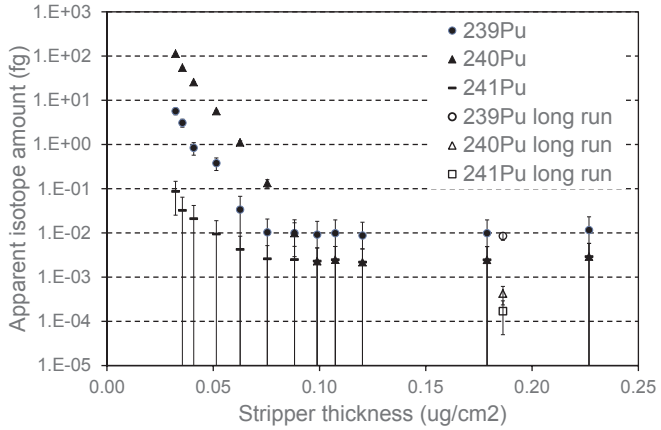

Fig. 8. Pu isotope amounts vs. stripper gas thickness for a ^{242}Pu spike sample.

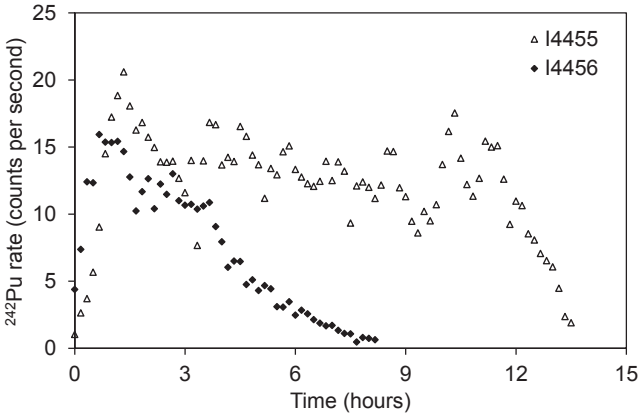

Fig. 9. Count rates observed for a pair of ^{242}Pu spike cathodes; each data point represents a run of 300 cycles with a 2.0 s cycle (0.1 s mass 239, 0.1 s 242, 1.8 s 244).

Table 4
Efficiency results for ^{242}Pu spike samples.

Sample ID	Binder	Overall efficiency	Ion source efficiency
I4455 + I4456	Nb	1.3%	3.2%
I4434	Nb	1.5%	3.9%
Pu-242A	no binder	0.6%	1.4%
Pu-242B	Ag	0.5%	1.2%
Pu-242C	no binder	0.4%	1.0%
Pu-242D	Ag	0.2%	0.5%

sensitivity (approximately 100 atoms). The calculated $^{244}Pu/^{242}Pu$ ratio of the material is 1.2×10^{-6}. The single count observed is likely due to ion source memory, due to use of a standard containing ^{244}Pu. Several further ^{242}Pu spike samples were run and the results are summarised in Table 4. While there is variability between samples, the results indicate that use of a niobium binder gives better performance than silver binder or loading samples without binder.

The standard (an in-house material containing ^{244}Pu) was run five times, briefly, in the course of the four day experiment, as a check of the system stability. No re-tuning or adjustment of the ion source was needed during the 4 days. The standard yielded a total of around 4000 ^{244}Pu atoms detected, sufficient that some source contamination could take place. While no standard has been run to exhaustion, in a separate experiment several samples containing Pu fallout were run to exhaustion (8 h per cathode) and the $^{240}Pu/^{239}Pu$ ratios were found to remain stable.

For measurement of ^{247}Cm in the same samples selected for ^{244}Pu analysis, it is planned to use ^{243}Am as a spike. Use of ^{244}Cm spike is undesirable as it could interfere with ^{244}Pu measurement if not separated completely. Information on the relative ionisation probability for Am and Cm has recently been published [29]. As a first step, the purity of the ^{243}Am spike has been checked to ensure it does not contain ^{244}Pu. To do this, double-spiked test cathodes were prepared with ^{240}Pu and ^{243}Am. With these cathodes we had the opportunity to test the overall efficiency and the relative ionisation probability for Pu and Am, again by running the samples to exhaustion. Derived average efficiencies are shown in Table 5; in Fig. 10 the count rates and the $^{240}Pu/^{243}Am$ ratios are plotted vs. the run number. The ratios start low, suggesting that the relative efficiencies (i.e. ionisation probabilities) change as the sample is consumed.

Table 5
Results from Am efficiency test samples.

Sample ID	Overall efficiency	Ion source efficiency	(Pu/Am) relative efficiency
I4517	0.80%	2.06%	1.38
I4518	0.91%	2.32%	*
I4519	0.77%	1.97%	1.33

* No added ^{240}Pu in this sample.

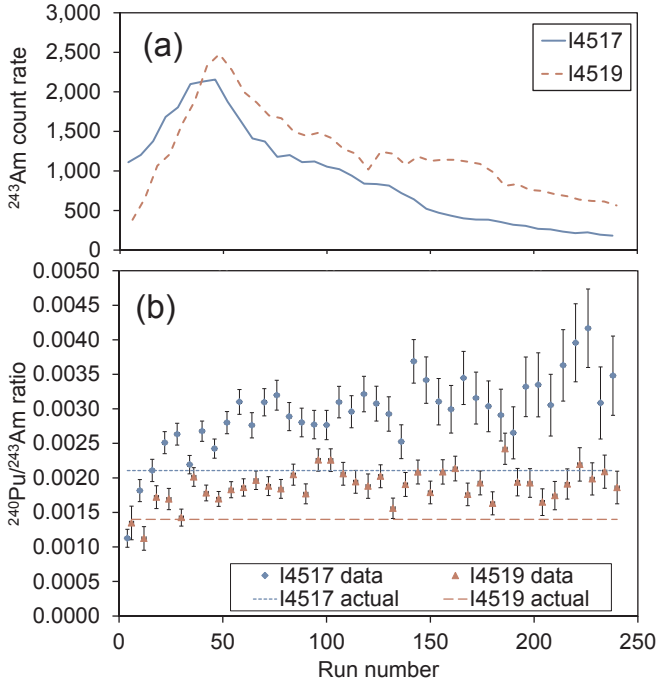

Fig. 10. (a) ^{243}Am count rate and (b) ^{240}Pu/^{243}Am ratio vs run number for the two double-spiked samples. The actual atom ratios of the samples are shown in (b).

7. Conclusion

The VEGA AMS system has been demonstrated to have excellent performance characteristics for actinides analysis. In particular, the charge state yield exceeds 40% for 3+ ions with helium stripping and the ion source efficiency can exceed 3% for extended running times on samples, leading to sub-attogram sensitivity in some cases, such as ^{240,241,244}Pu. The system has a high degree of flexibility, enabling quasi-simultaneous analysis of up to eight rare isotopes and additionally several higher-abundance species, utilising three isotope detection methods in parallel. For uranium isotopes, isotope ratio precisions better than 1% are possible. With careful control of sources of uranium background, accuracies at the 1% level should be achievable in future. The system is used in a wide range of applications, for U and Pu isotopic analysis, and has additionally been applied to measurements of ^{129}I, Pt stable isotopes and Pb isotopes.

Acknowledgments

We acknowledge the financial support from the Australian Government for the Centre for Accelerator Science at ANSTO through the National Collaborative Research Infrastructure Strategy (NCRIS).

References

[1] M.A.C. Hotchkis, D.P. Child, B. Zorko, Actinides AMS for nuclear safeguards and related applications, Nucl. Instrum. Methods B 268 (2010) 1257–1260.
[2] M. Hotchkis, D. Child, K. Wilcken, Applications of accelerator mass spectrometry in nuclear verification, JNMM-J. Inst. Nucl. Mater. Manag. 40 (2012) 60–68.
[3] M.J. Kristo, E. Keegan, M. Colella, R. Williams, R. Lindvall, G. Eppich, S. Roberts, L. Borg, A. Gaffney, J. Plaue, K. Knight, E. Loi, M. Hotchkis, K. Moody, M. Singleton, I. Hutcheon, Nuclear forensic analysis of uranium oxide powders interdicted in Victoria, Australia, Radiochim. Acta 103 (2015) 487–500.
[4] S.F. Boulyga, A. Koepf, S. Konegger-Kappel, Z. Macsik, G. Stadelmann, Uranium isotope analysis by MC-ICP-MS in sub-ng sized samples, JAAS 31 (2016) 2272–2284.
[5] M.P. Johansen, D.P. Child, E. Davis, C. Doering, J.J. Harrison, M.A.C. Hotchkis, T.E. Payne, S. Thiruvoth, J.R. Twining, M.D. Wood, Plutonium in wildlife and soils at the Maralinga legacy site: persistence over decadal time scales, J. Environ. Radioact. 131 (2014) 72–80.
[6] D.P. Child, M.A.C. Hotchkis, Plutonium and uranium contamination in soils from former nuclear weapon test sites in Australia, Nucl. Instrum. Methods B 294 (2013) 642–646.
[7] J.J. Harrison, T.E. Payne, K.L. Wilsher, S. Thiruvoth, D.P. Child, M.P. Johansen, M.A.C. Hotchkis, Measurement of ^{233}U/^{234}U ratios in contaminated groundwater using alpha spectrometry, J. Environ. Radioact. 151 (2016) 537–541.
[8] B.S. Smith, D.P. Child, D. Fierro, J.J. Harrison, H. Heijnis, M.A.C. Hotchkis, M.P. Johansen, S. Marx, T.E. Payne, A. Zawadzki, Measurement of fallout radionuclides, ^{239,240}Pu and ^{137}Cs, in soil and creek sediment: Sydney Basin, Australia, J. Environ. Radioact. 151 (2016) 579–586.
[9] M.P. Johansen, D.P. Child, E.A. Caffrey, E. Davis, J.J. Harrison, M.A.C. Hotchkis, T.E. Payne, A. Ikeda-Ohno, S. Thiruvoth, J.R. Twining, N.A. Beresford, Accumulation of plutonium in mammalian wildlife tissues following dispersal by accidental-release tests, J. Environ. Radioact. **151** (2016) 387–394.
[10] M.B. Froehlich, M.M.A. Dietze, S.G. Tims, L.K. Fifield, A comparison of fallout ^{236}U and ^{239}Pu uptake by Australian vegetation, J. Environ. Radioact. 151 (2016) 558–562.
[11] H.G. Smith, G.J. Sheridan, P. Nyman, D.P. Child, P.N.J. Lane, M.A.C. Hotchkis, G.E. Jacobsen, Quantifying sources of fine sediment supplied to post-fire debris flows using fallout radionuclide tracers, Geomorph. 139–140 (2012) 403–415.
[12] E. Field, S. Marx, J. Haig, J.-H. May, G. Jacobsen, A. Zawadzki, D. Child, H. Heijnis, M. Hotchkis, H. McGowan, P. Moss, Untangling geochronological complexity in organic spring deposits using multiple dating methods, Quat. Geochronol. 43 (2018) 50–71.
[13] C. Woodward, J. Shulmeister, A. Zawadzki, D. Child, L. Barry, M. Hotchkis, Holocene ecosystem change in Little Llangothlin Lagoon, Australia: implications for the management of a Ramsar-listed wetland, Hydrobiologia 785 (2017) 337–358.
[14] S.K. Marx, J.M. Knight, P.G. Dwyer, D.P. Child, M.A.C. Hotchkis, J.M. Olley, A. Zawadzki, Living landscapes: ecogeomorphic feedbacks allow mangroves to respond to sea level rise, to be published, 2018.
[15] A. Wallner, T. Faestermann, J. Feige, C. Feldstein, K. Knie, G. Korschinek, W. Kutschera, A. Ofan, M. Paul, F. Quinto, G. Rugel, P. Steier, Abundance of live ^{244}Pu in deep-sea reservoirs on Earth points to rarity of actinide nucleosynthesis, Nat. Commun. 6 (2015) 5956.
[16] A. Wallner, N. Kinoshita, M. Froehlich, M. Hothchkis, M. Paul, K. Fifield, S. Pavetich, S. Tims, The unknown site of r-process nucleosynthesis – clues from extraterrestrial ^{244}Pu and ^{247}Cm? 14th International Conference on Accelerator Mass Spectrometry, Ottawa, Canada, (2017).
[17] K. Wilcken, M. Hotchkis, V. Levchenko, D. Fink, T. Hauser, R. Kitchen, From carbon to actinides: A new universal 1MV accelerator mass spectrometer at ANSTO, Nucl. Instrum. Methods B 361 (2015) 133–138.
[18] National Electrostatics Corporation, Wisconsin, USA, http://www.pelletron.com.
[19] C. Vockenhuber, V. Alfimov, M. Christl, J. Lachner, T. Schulze-König, M. Suter, H.A. Synal, The potential of He stripping in heavy ion AMS, Nucl. Instrum. Methods B 294 (2013) 382–386.
[20] S.R. Winkler, P. Steier, J. Buchriegler, J. Lachner, J. Pitters, A. Priller, R. Golser, He stripping for AMS of ^{236}U and other actinides using a 3MV tandem accelerator, Nucl. Instrum. Methods B 361 (2015) 458–464.
[21] A.B. Wittkower, H.D. Betz, Equilibrium charge-state distributions of 2–15-MeV tantalum and uranium ions stripped in gases and solids, Phys. Rev. A 7 (1973) 159–167.
[22] James F. Ziegler, SRIM – The Stopping and Range of Ions in Matter, http://www.srim.org/.
[23] ETP Ion Detect, Sydney, Australia, https://www.etp-ms.com/.
[24] J. Lachner, M. Christl, C. Vockenhuber, H.-A. Synal, Detection of UH^{3+} and ThH^{3+} molecules and 236U background studies with low-energy AMS, Nucl. Instrum. Methods B 294 (2013) 364–368.
[25] K.M. Wilcken, L.K. Fifield, T.T. Barrows, S.G. Tims, L.G. Gladkis, Nucleogenic ^{36}Cl, ^{236}U and ^{239}Pu in uranium ores, Nucl. Instrum. Methods. B 266 (2008) 3614–3624.
[26] J.R. Southon, G.M. Santos, Ion source development at KCCAMS, University of California, Irvine, Radiocarbon 46 (2004) 33–39.
[27] J. Southon, G.M. Santos, Life with MC-SNICS. Part II: further ion source development at the Keck carbon cycle AMS facility, Nucl. Instrum. Methods B 259 (2007) 88-–93.
[28] B.X. Han, J.R. Southon, M.L. Roberts, K.F. von Reden, Computer simulation of MC-SNICS for performance improvements, Nucl. Instrum. Methods B 261 (2007) 588–593.
[29] M. Christl, X. Dai, J. Lachner, S. Kramer-Tremblay, H.-A. Synal, Low energy AMS of americium and curium, Nucl. Instrum. Methods B 331 (2014) 225–232.